Received: 13 November 2024 | Revised: 8 January 2025 | Accepted: 15 January 2025

DOI: 10.1096/fj.202402842R

RESEARCH ARTICLE

The FASEB Journal

Dysregulated fatty acid metabolism in pericardiac adipose tissue of pulmonary hypertension due to left heart disease mice

Haihua Qiu[1] | Jingyuan Chen[1] | Zhang Mei[2] | Wenjie Chen[1] | Luo Jun[1] | Yusi Chen[1] | Yingjie Tan[1] | Tianyu Wang[1] | Yaqin Chen[1] | Jiang Li[1]

[1]Department of Cardiovascular Medicine, Second Xiangya Hospital of Central South University, Changsha, Hunan, China

[2]Xiangya School of Nursing of Central South University, Changsha, Hunan, China

Correspondence
Jiang Li, Department of Cardiovascular Medicine, Second Xiangya Hospital of Central South University, No. 139 Middle Renmin Road, Furong District Changsha, Hunan 410011, China.
Email: lijiangcs@csu.edu.cn

Funding information
National Nature Science Foundation of China, Grant/Award Number: 82470055; Hunan Provincial Nature Science Foundation of China, Grant/Award Number: 2022JJ30067 and 2023JJ40811; Fundamental Research Funds for the Central Universities of Central South University, Grant/Award Number: 2024ZZTS0534

Abstract

Pulmonary hypertension associated with left heart disease (PH-LHD) represents the most prevalent form of pulmonary hypertension; however, being lacks precise and effective treatment strategies. Recent clinical studies have indicated a positive correlation between the volume of pericardiac adipose tissue (PAT) and the severity of PH-LHD. Nonetheless, there is a paucity of research characterizing PAT phenotypes in PH-LHD disease models. This study aimed to elucidate the gene-level characteristics of PAT in PH-LHD through RNA sequencing and targeted metabolomic analysis of PAT in order to identify potential therapeutic targets for PH-LHD by modulating PAT. This study developed a mouse model of PH-LHD through cardiac overload combined with metabolic syndrome and verified that PAT volume and adipocyte size were significantly increased in PH-LHD mice. We used RNA sequencing to reveal that DEGs in PAT were primarily enriched in fatty acid metabolism pathways. Then, real-time PCR showed no significant differences in the mRNA expression of inflammatory markers or adipocytokines; however, genes of fatty acid synthesis (Fasn, Acaca, and Scd1) and fatty acid decomposition (Ehhadh, Acot4, and Pdk1) significantly changed between the two groups. Consistently, targeted metabolomic analysis showed levels of most types of medium- and long-chain fatty acids substantially reduced in PAT, suggesting that PAT in PH-LHD mice exhibits suppressed fatty acid de novo synthesis and enhanced fatty acid breakdown, resulting in impaired fatty acid storage. These findings highlight the potential of targeting PAT fatty acid synthesis and metabolism pathways as a novel therapeutic approach for PH-LHD.

KEYWORDS

fatty acid metabolism, Pericardiac adipose tissue, pulmonary hypertension due to left heart disease

Haihua Qiu and Jingyuan Chen contributed equally to this work.

1 | INTRODUCTION

Pulmonary hypertension (PH) due to left heart disease (PH-LHD) is classified as Group 2 PH and arises from various forms of left heart failure, including systemic hypertension and valvular heart disease.[1] Despite advances in understanding, effective treatments for PH-LHD remain elusive. The diagnostic criteria and clinical categorization of PH-LHD phenotypes are still evolving, posing challenges for basic and translational research focused on this condition. The underlying pathophysiology involves elevated left-sided filling pressures, which lead to passive backward transmission of increased pressures to the pulmonary vasculature.[2] PH is recognized as a significant risk factor and a predictor of poor outcomes in patients with LHD.[3,4] Risk factors such as advanced age, obesity, coronary microvascular disease, chronic obstructive pulmonary disease (COPD), and atrial fibrillation are associated with a higher incidence of PH in the setting of LHD.[5] Recent studies have highlighted that the most critical determinants of pulmonary hemodynamics in PH-LHD are left heart remodeling and fibrosis, as well as elevated left ventricular end-diastolic pressure, all of which are closely linked to the development of PH.[6]

Pericardial adipose tissue (PAT), which includes both epicardial adipose tissue (EAT) and para-pericardial adipose tissue, is increasingly recognized for its role in cardiovascular disease.[7] PAT acts as a metabolically active, endocrine organ capable of producing free fatty acids and various pro- and anti-inflammatory adipocytokines, contributing to diverse cardiovascular pathologies.[8] Elevated PAT thickness has been associated with increased systolic blood pressure, higher incidence of diabetes, dyslipidemia, overweight, and coronary artery calcification in patients with coronary artery disease (CAD).[9] Furthermore, increased PAT is linked to subclinical changes in left ventricular structure and function, such as a higher left ventricular mass index and impaired systolic function, independent of overall or abdominal obesity indices.[9] These findings suggest that PAT may influence cardiac structure and hemodynamics, potentially exacerbating PH in the context of LHD. Notably, in patients with LHD, an increased EAT, one component of PAT, has been associated with elevated mean pulmonary artery pressure (mPAP), right atrial pressure (RAP), and pulmonary capillary wedge pressure (PCWP), suggesting that PAT may be a significant risk factor for PH.[10,11] In this study, we investigated the phenotype of PAT through morphological, pathological, and molecular analyses using an animal model of PH-LHD, aiming to elucidate the pathophysiological mechanisms by which PAT influences cardiac remodeling and pulmonary vascular remodeling.

2 | METHOD

2.1 | Animal studies

In this study, we used abdominal aorta banding (AAB) to induce pressure overload and a combination of high-fat diet (HFD) and olanzapine to induce metabolic syndrome (MetS), together establishing the PH-LHD model, as previously described.[12,13] In brief, male Swiss mice (30 ± 2 g) were anesthetized with 2% isoflurane. In the left lateral position, 1–2 cm longitudinal incision was cut 1 cm below the last left rib near the spine, exposing and carefully separating the abdominal aorta. A blunt 27-gauge needle (outer diameter 0.4 mm) was used to standardize the constriction of the abdominal aorta. The vessel was ligated with 6–0 silk wire. The success of the constriction was determined by the kidney color changing from pink to pale; immediately draw the blunt needle, and the kidney was visible again to pink.

MetS was induced by a high-fat diet (60% fat, D12492, BIOPIKE, China) and olanzapine (4 mg/kg/2 days, intraperitoneally, S2493, Selleck, China). Swiss mice were randomly divided into 2 groups ($n = 10$–15 in each group): (1) Control group (sham operation), (2) PH-LHD group (AAB + MetS). Relation measures of PH-LHD identification were assessed in each group at the end of week 10. All animal care and experiments were approved by the Animal Research Committee of Central South University in Hunan, China. All animals were purchased from Hunan SJA Laboratory Animal Co., Ltd., (License No. SCXK (Xiang) 2019-0004).

2.2 | Transthoracic echocardiography

Transthoracic echocardiography was performed at the end of the study to assess the structural and functional parameters of the left ventricle (LV) and right ventricle (RV). Mice were anesthetized with 2% isoflurane, and echocardiographic measurements were obtained by skilled technicians using the Vevo 770 System (VisualSonics, ON, Canada). Parameters assessed included end-diastolic thickness of left ventricular posterior wall (LVPWd), end-diastolic interventricular septal thickness (IVSd), left ventricular ejection fraction (LVEF), the ratio of early diastolic mitral annular velocity and mitral peak velocity of late filling (E/A), pulmonary artery acceleration time (PAAT), tricuspid annular

plane systolic excursion (TAPSE), and right ventricular end-diastolic diameter (RVDd), following previously established protocols.[14] Additionally, pericardial adipose tissue (PAT) thickness was measured as described in earlier studies.[10]

2.3 | Hemodynamics assessment

Mice were anesthetized with 2% isoflurane and endotracheally intubated. Right ventricular systolic pressure (RVSP) was measured using a PE-50 catheter (0.58 mm inner diameter, 0.96 mm outer diameter) inserted into the right ventricle (RV) via the jugular vein, following the procedure outlined in our previous study.[15] Subsequently, a right thoracotomy was performed, and the apex of the left ventricle (LV) was punctured with a 22-gauge needle connected to a pressure transducer. Left ventricular systolic pressure (LVSP) and left ventricular end-diastolic pressure (LVEDP) were continuously recorded for 3–5 min using the RM6240E data acquisition system (Chengdu Instrument Factory, China).

2.4 | Histology of heart and lungs

After hemodynamic evaluation, heart and lung tissue of the mice were harvested, fixed by 4% paraformaldehyde and paraffin-embedded. The lung sample was stained with hematoxylin and eosin (HE) (Servicebio, Wuhan, China) to evaluate pulmonary vascular remodeling. Pulmonary vascular thickness was calculated as wall thickness (WT, %) = (external diameter–internal diameter)/external diameter × 100%.

The heart and adjacent PAT sample stained with HE to evaluate not only the cardiac structural disorders but also observe PAT morphology. Adipocyte area was measured by image J software (three microscopic fields per sample, ×630 magnification). The volume of an adipocyte = (4/3)*(3.14*√(Area/3.14) 3), and using the formula (Adipocyte volume/Average adipocyte volume of the control group) * 100, we can determine the percentage change in adipocyte volume. In addition, we also compared the adipocyte volume of two groups through assessing adipocyte size distribution.

2.5 | RNA sequencing and analysis

A global analysis of PAT gene expression was performed by total RNA sequencing. Total RNA was extracted with TRIzol reagent (Invitrogen, USA). RNA quality was assessed by measuring the RNA integrity number (RIN) using a Fragment Analyzer HS Total RNA Kit (Advanced Analytical Technologies, Inc.). The sequencing data was filtered with SOAPnuke (v1.5.2), and clean reads were obtained and stored in FASTQ format. The clean reads were loaded into the BGI Dr. Tom platform and analyzed with DESeq2 (v1.4.5). Genes with adjusted values of $p < .05$ and $|\log_2 FC| > 2.0$ were deemed to be differentially expressed genes (DEGs). The data were analyzed on the online platform of the Majorbio Cloud Platform (www.majorbio.com).

2.6 | Metabolomic analysis of medium- and long- chain fatty acids

To determine the composition of PAT fatty acids, fatty acid metabolites were analyzed by targeted metabolomics. The weight of >30 mg per sample for targeted metabolomic analysis of medium- and long-chain fatty acids. The samples were lysed by sonication using 5 mL of chloroform/methanol (1:2, v/v). The supernatant was collected, 2 mL of H2SO4/methanol solution (1:99, v/v) and an internal standard were added for methyl esterification, and the methyl esters were extracted with 2 mL of hexane. The injection volume was 1 μL, with a split injection ratio of 1:10, for the Gas chromatography–mass spectrometry (GC–MS) test.

GC–MS was performed using an Agilent 7890B gas chromatograph coupled to an Agilent 5977B mass spectrometer. The chromatography was performed with a gas chromatography capillary column (30 m × 250 μm × 0.25 μm, Agilent 19091S-433UI:HP-5 ms). The temperature was programmed as follows: initial hold at 80°C; gradually increased to 180°C at a rate of 20°C/min and held at 180°C for 8 min; then gradually increased to 280°C at a rate of 5°C/min and held at 280°C for 3 min. Helium was used as the carrier gas at a flow rate of 1.0 mL/min. To evaluate the stability and reproducibility of the detection system, QC samples (pooled from all samples) were analyzed. The mass spectrometry conditions were as follows: the injection port, ion source, and transfer line temperature were set to 280°C, 230°C, and 250°C, respectively; the electron bombardment was the electron impact ionization source with 70 eV ionizing energy in selected ion monitoring scanning mode. The mass data were analyzed using MSD ChemStation software (Agilent Technologies) to extract the chromatographic peak area and retention time. Finally, a standard curve was generated, and the individual fatty acid concentrations of each sample were calculated. The complete platform and fatty acid methyl ester mixed standard solutions were provided by Shanghai Applied Protein Technology Company, Ltd.

TABLE 1 Primer sequences for RT-PCR.

Genes		Sequences
IL-1b	Forward	GAAATGCCACCTTTTGACAGTG
	Reverse	TGGATGCTCTCATCAGGACAG
IL-6	Forward	GTCCTTCCTACCCCAATTTCCA
	Reverse	TAACGCACTAGGTTTGCCGA
TNFα	Forward	ACTGAACTTCGGGGTGATCG
	Reverse	TGGTGGTTTGTGAGTGTGAGG
AdipoQ	Forward	AGCCGCTTATGTGTATCGCT
	Reverse	GAGTCCCGGAATGTTGCAGT
Leptin	Forward	GGCTCAGGACATTCCAGCTT
	Reverse	AAGGCATAGGAGAAGCCCGTG
PPARγ	Forward	GAGGGACGCGGAAGAAGAG
	Reverse	CACAGGCTCCTGTCAGAGTG
Fasn	Forward	GGAGGTGGTGATAGCCGGTAT
	Reverse	TGGGTAATCCATAGAGCCCAG
Acaca	Forward	AATGAACGTGCAATCCGATTTG
	Reverse	ACTCCACATTTGCGTAATTGTTG
Scd1	Forward	TTCTTGCGATACACTCTGGTGC
	Reverse	CGGGATTGAATGTTCTTGTCGT
Ehhadh	Forward	GTTTGGACCATACGGTTAGAGC
	Reverse	GCTTCTGGTATCGCTGTATTTCA
Acot4	Forward	GCAGTGCGGTACATGCTTC
	Reverse	AGAGCCATTGATGGAAACTGTG
Pdk4	Forward	CCGCTTAGTGAACACTCCTTC
	Reverse	TGACCAGCGTGTCTACAAACT
β-Actin	Forward	GGCTGTATTCCCCTCCATCG
	Reverse	CCAGTTGGTAACAATGCCATGT

2.7 | Real-time quantitative PCR

RNA extraction and real-time quantitative PCR were performed as previously described.[15] The sequences of the primer pairs used in this study were listed as follows. Data were normalized to beta-actin and expressed as a relative ratio. Primer sequences for RT-PCR are as follows (Table 1).

3 | RESULTS

3.1 | Combination of MetS and AAB induces PH-LHD mice

Compared with Sham controls, mice with PH-LHD exhibited significant left ventricular (LV) hypertrophy and diastolic dysfunction, evidenced by an increased end-diastolic posterior wall thickness (LVPWd), increased end-diastolic interventricular septal wall thickness (IVSd), and a reduced E/A ratio (Figure 1A–E). Notably, the left ventricular ejection fraction (LVEF) remained unchanged between the control and model groups.

Consistent with previous studies, metabolic syndrome (MetS) combined with abdominal aortic banding (AAB) further aggravated right ventricular (RV) dysfunction in PH-LHD mice. This was reflected by a reduction in pulmonary artery acceleration time (PAAT) and tricuspid annular plane systolic excursion (TAPSE), alongside a significant increase in right ventricular end-diastolic diameter (RVDd) (Figure 1F–I). Specifically, PAAT decreased from 25 ms in controls to 18.3 ms in the PH-LHD group, while TAPSE dropped from 1.35 mm to 0.83 mm (Figure 1G,H). Conversely, RVDd increased from 2.18 mm in control mice to 3.06 mm in PH-LHD mice (Figure 1I).

In addition, PH-LHD mice demonstrated worsened hemodynamic parameters compared to Sham controls, including elevated right ventricular systolic pressure (RVSP) and left ventricular end-diastolic pressure (LVEDP) (Figure 2A–C). The RVSP in the PH-LHD group was 33.7 mmHg, compared to 17.8 mmHg in the control group (Figure 2B). Similarly, LVEDP, a more precise indicator of LV diastolic function, was 9.5 mmHg in the PH-LHD group, compared to 4.7 mmHg in control mice (Figure 2C). Moreover, substantial pulmonary vascular remodeling was evident in PH-LHD mice, with histological analysis showing an increase in pulmonary vascular wall thickness (VWT, %) from 17.2% in controls to 47.4% in the PH-LHD group (Figure 2D,E).

3.2 | PAT increased significantly in the PH-LHD mouse model

To investigate the changes in PAT, the thickness of PAT at the left ventricular apex was measured using echocardiography. The results demonstrated that PAT thickness was significantly greater in the PH-LHD group compared to the control group (Figure 3A,B). Consistently, after sacrifice, the wet weight of PAT was measured, and the ratio of PAT weight to body weight was calculated for each group. The PAT-to-body weight ratio was 0.166 mg/g in the control group, increasing to 0.477 mg/g in the PH-LHD group, indicating a significant increase in PAT in the PH-LHD mouse model (Figure 3A,C).

Furthermore, HE staining of PAT was performed, followed by a quantitative analysis of adipocyte size in both groups (Figure 3D). The analysis revealed that the average adipocyte volume in the PH-LHD group was 10.5 times greater than that in the control group (Figure 3E). To better illustrate the differences in PAT between PH-LHD and

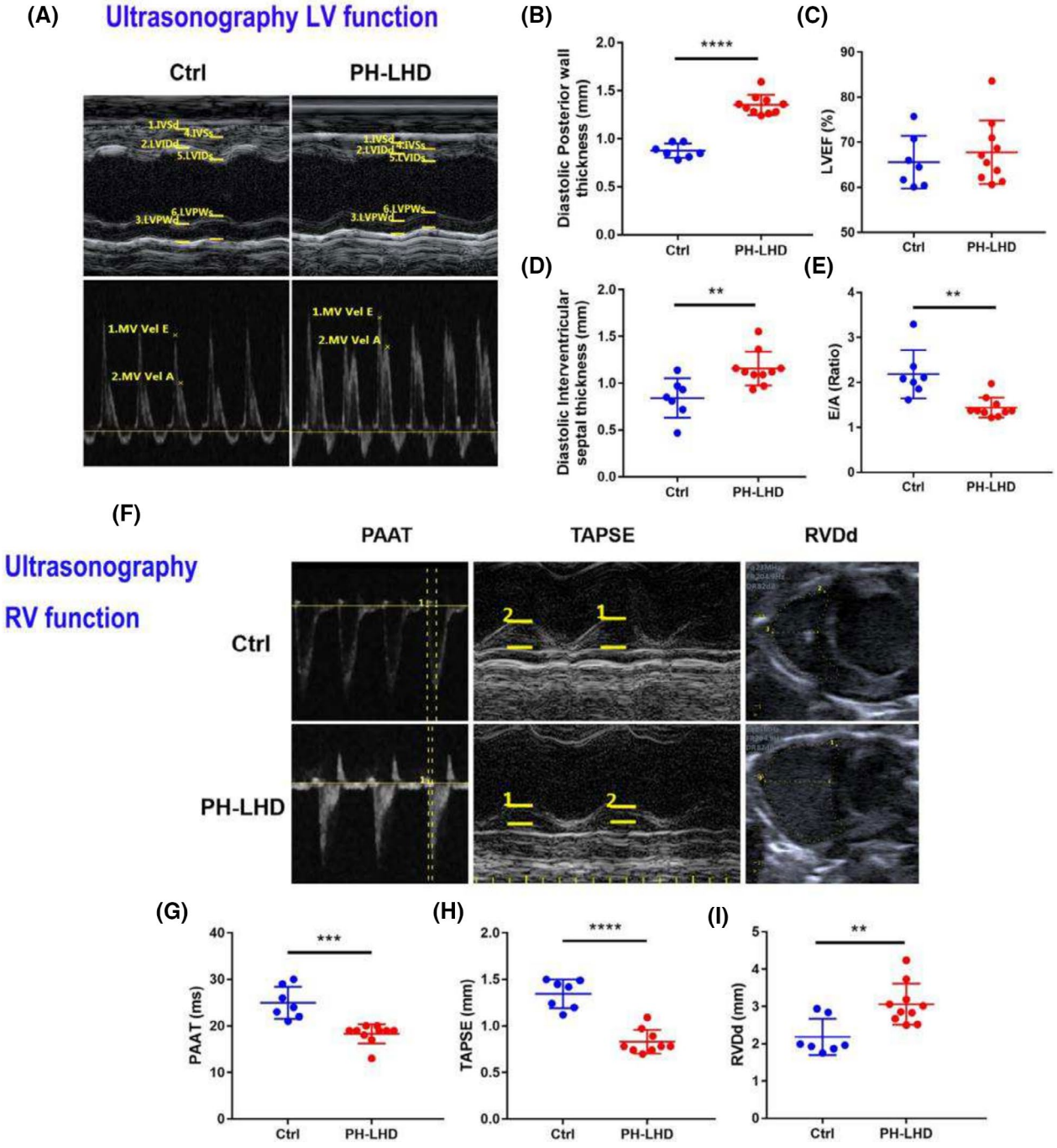

FIGURE 1 LV and RV structural damage and dysfunction in PH-LHD models induced by a combination of MetS and AAB. (A) Representative images from M mode and pulse-wave (PW) doppler mode ultrasonography. (B–E) Statistical analysis of end-diastolic posterior wall (LVPWd), end-diastolic left ventricular Ejection fraction (LVEF), end-diastolic interventricular septal wall thickness (IVSd), and E wave/A wave ratio (E/A) ($n = 7$~10). (F) Representative images of M mode and PW doppler mode ultrasonography used to calculate pulmonary artery acceleration time (PAAT), tricuspid annular plane systolic excursion (TAPSE), and right ventricular end-diastolic diameter (RVDd). (G–I) Statistical analysis of PAAT, TAPSE and RVDd ($n = 7$~10). ****$p < .0001$, ***$p < .001$, **$p < .01$, PH-LHD vs. Ctrl group.

control mice, the distribution of adipocyte volumes was assessed. In PH-LHD mice, the majority of adipocytes were concentrated in larger volume regions, whereas in control mice, adipocytes were predominantly found in smaller volume regions (Figure 3F).

3.3 | The results of RNA sequencing in PAT of PH-LHD mice

To further investigate the phenotype of increased PAT in PH-LHD mice and identify potential therapeutic targets

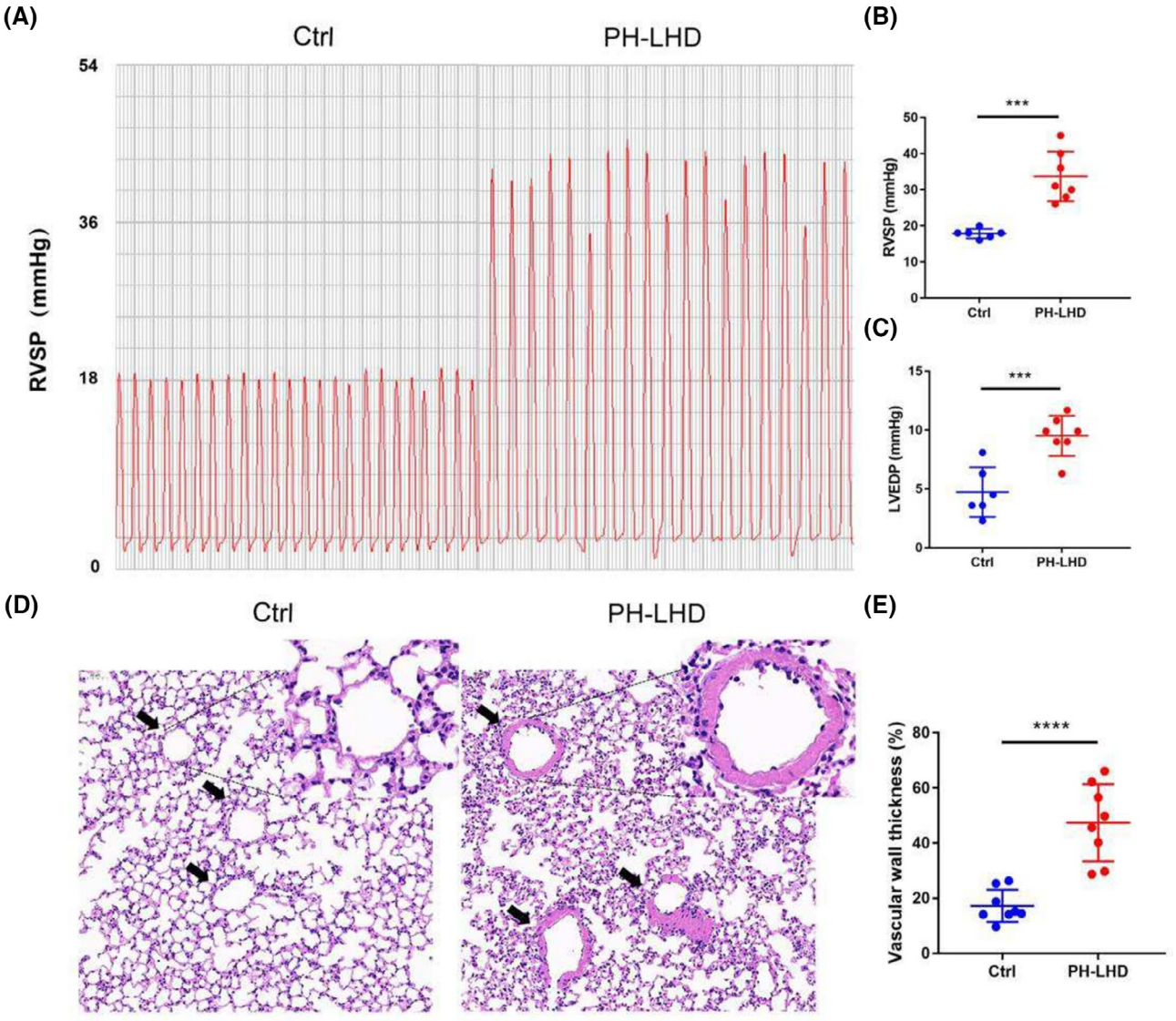

FIGURE 2 Hemodynamic disorder and pulmonary vascular remodeling in PH-LHD mice. (A) RVSP measurement in experimental mice. (B, C) Statistical analysis of RVSP and LVEDP ($n = 6$~7). (D) Representative images of HE-stained lung sections under a light microscope in each group, the black arrow points to pulmonary vessels, and the enlarged vessel is presented in the upper right corner. The pathological sections of lung tissue were scanned and analyzed by Caseviewer software (3DHISTECH, Hungary, ×200 magnification, scale bars: 50 μM). (E) Statistical analysis of pulmonary vascular wall thickness (VWT, %) ($n = 8$). LVEDP, left ventricular end-diastolic pressure; RVSP, right ventricular systolic pressure. ****$p < .0001$, ***$p < .001$, PH-LHD vs. Ctrl group.

for PH-LHD, we performed bulk RNA sequencing to profile transcriptomes and overrepresented gene ontologies in mice subjected to PH-LHD compared with controls. RNA sequencing of PAT revealed 145 differentially expressed genes (DEGs) between the two groups, with 69 genes upregulated and 76 genes downregulated in the PH-LHD group compared to controls (Table S1). The heatmap and volcano plot illustrated the distribution and range of expression changes of DEGs between the PH-LHD and Sham control groups (Figure 4A,B).

Among the 145 significantly altered genes, the top 10 most upregulated genes in the PH-LHD group included Mageb18, Tm4sf19, Slc5a7, Ccdc7a, Usp29, Mmp12, Duox1, Zim1, Cyp4a32, and Chrna2. The top 10 downregulated genes were Slc2a5, Pde6a, Cyp1a, Fasn, St6galnac1, Atp4b, Scd1, Acaca, Serpina3m, and Cd177. Gene Ontology (GO) enrichment analysis of these DEGs revealed key biological processes and pathways potentially involved in PH-LHD. The significantly represented biological processes in the PAT transcriptome included fatty acid metabolic processes, regionalization,

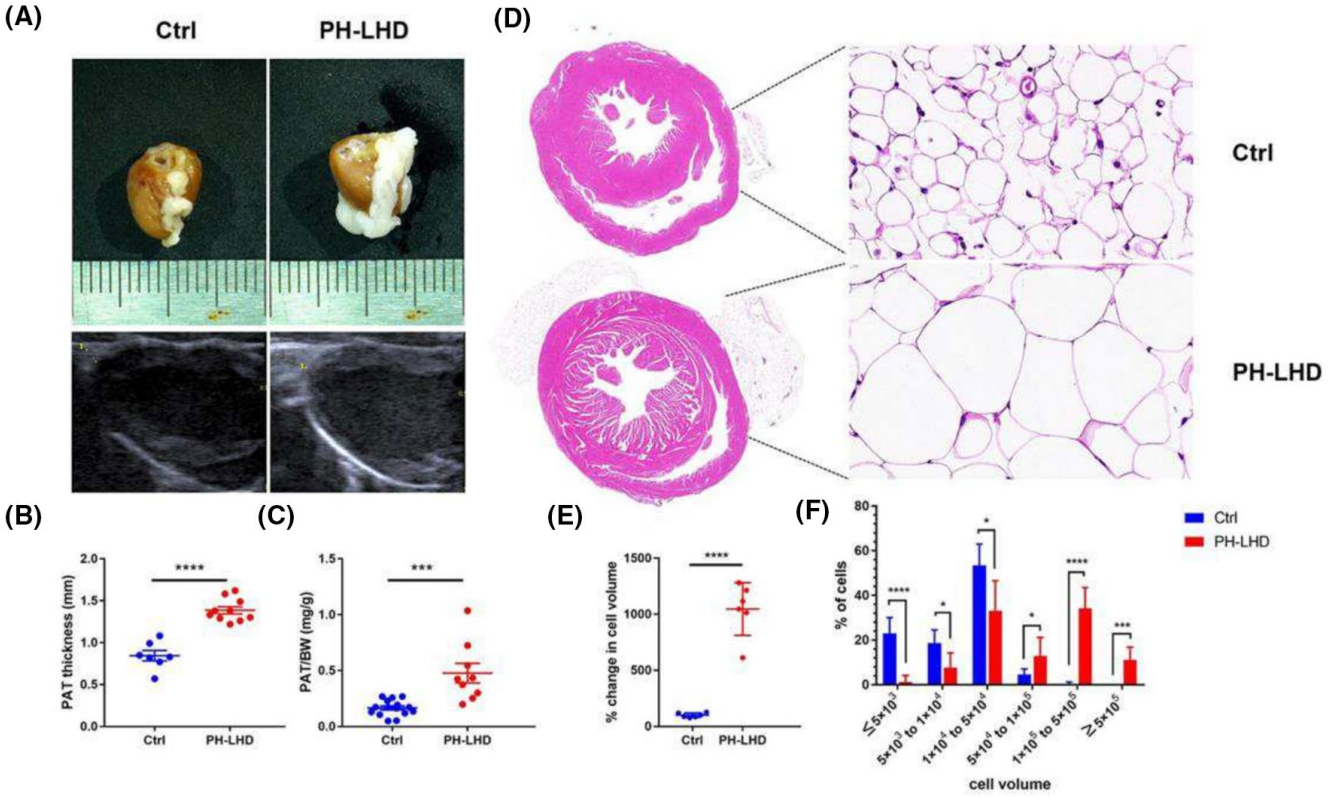

FIGURE 3 PAT increased in PH-LHD mice. (A) Representative images of heart and adjacent PAT samples in different groups and representative images of PAT thickness measured by transthoracic echocardiography. (B) Statistical analysis of PAT thickness ($n = 7$~10). (C) Statistical analysis of wet weight of PAT to body weight ($n = 9$~15). (D) Representative images of HE-stained heart and adjacent PAT sections under a light microscope, the enlarged adipocyte is presented on the right. (E) Statistical analysis of the percentage change in cell volume. (F) cell volume distribution of PAT in the ctrl and PH-LHD group mice ($n = 6$). The pathological sections of PAT were scanned and analyzed by Caseviewer software (3DHISTECH, Hungary, ×630 magnification, scale bars:20 μM. ****$p < .0001$, ***$p < .001$, *$p < .05$, PH-LHD vs. Ctrl group.

and responses to extracellular stimuli. Enrichment analysis of GO cellular components indicated that many of these genes were localized to asymmetric synapses, receptor complexes, and postsynaptic densities (Figure 4C).

Pathway analysis using KEGG mapping indicated that these DEGs were involved in several pathways, including PPAR signaling pathway, Phagosome, Asthma, Allograft rejection, Graft-versus-host disease, Type I diabetes mellitus, Autoimmune thyroid disease, Cell adhesion molecules, Viral myocarditis, Antigen processing and presentation, Rheumatoid arthritis, Intestinal immune network for IgA production, Cholesterol metabolism, Fatty acid biosynthesis, Glycerolipid metabolism (Figure 4D). Notably, genes encoding key enzymes involved in fatty acid synthesis, such as fatty acid synthase (Fasn), acetyl-CoA carboxylase alpha (Acaca), and stearoyl-CoA desaturase 1 (Scd1), were consistently downregulated in the PAT of PH-LHD mice. Additionally, protein–protein interaction (PPI) analysis identified four DEGs with the highest interaction scores (interaction score > 0.95), primarily associated with fatty acid synthesis and metabolism (Figure 4E).

3.4 | Fatty acid synthesis and metabolism-related genes were significantly differentially expressed in PAT of PH-LHD mice

Previous studies have suggested that pericardial adipose tissue (PAT) may exacerbate cardiovascular diseases, such as coronary heart disease and heart failure, by secreting adipokines and promoting inflammation. To investigate this further, we assessed the mRNA expression of classical inflammatory markers in the PAT of the PH-LHD mouse model. Contrary to expectations, real-time PCR analysis revealed no significant differences in the mRNA expression levels of IL-1β, IL-6, and TNF-α between the PH-LHD and control groups (Figure 5A–C).

We then examined the mRNA expression of both protective and harmful adipokines in PAT, including

adiponectin, leptin, and PPARγ. The expression levels of adiponectin and leptin showed no significant differences between the two groups (Figure 5D,E). However, PPARγ mRNA expression was significantly elevated, being 1.65 times higher in the PH-LHD group compared to controls (Figure 5F).

Subsequently, we analyzed the mRNA expression levels of key enzymes involved in fatty acid synthesis and metabolism in PAT. Consistent with our RNA sequencing data, the mRNA expression levels of key enzymes involved in fatty acid de novo synthesis, such as Fasn, Acaca, and Scd1, were significantly reduced in the PH-LHD group, showing reductions of 7.55, 5.34, and 5.65 times, respectively, compared to the control group (Figure 5G–I). Conversely, the mRNA expression of enzymes involved in fatty acid catabolism, including Ehhadh, Acot4, and Pdk4, was significantly increased in the PH-LHD group, by 3.55, 1.94, and 2.42 times, respectively, compared to controls (Figure 5J–L). These findings suggest that fatty acid storage in PAT is markedly impaired in PH-LHD mice, as the de novo synthesis of fatty acids is suppressed while fatty acid breakdown is enhanced.

3.5 | Changes of medium- and long-chain fatty acids in PAT of PH-LHD mice

The gas chromatography-tandem mass spectrometry system was employed to analyze the lipid profiles of pericardiac adipose tissue based on the single ion/selective ion monitoring technology (SIM). The contents of various medium- and long-chain fatty acids (>6 carbon atoms) in PAT were detected. In this result, lipids with variable importance values >1, mean fold change >1.5, and $p < .05$ were visualized in a heat map (Figure 6A). Compared to the control group, the levels of most medium- and long-chain fatty acids in the PAT of PH-LHD mice were significantly decreased, except for stearic acid (C18:0), oleic acid (C18:1N9), and elaidic acid (C18:1TN9), which were elevated in the PH-LHD group (Figure 6C–M). Notably, the total polyunsaturated fatty acid (PUFA) content in PH-LHD mice was 1.6 times lower than in controls (Figure 6F). Overall, the predominant downregulation of medium- and long-chain fatty acids in the PAT of PH-LHD mice is consistent with decreased de novo fatty acid synthesis (Figure 6B).

4 | DISCUSSION

In LHD-PH, the underlying conditions are often complex and include coronary artery disease (CAD), hypertension, and various forms of valvular heart disease leading to heart failure. Among these conditions, patients with PH who also present with obesity and metabolic syndrome constitute a significant subset.[16] The presence of both metabolic syndrome and obesity is associated with a more severe PH phenotype.[17] Animal models for studying LHD-PH are diverse.[18] In our study, we successfully established an LHD-PH model using a combination of HFD, olanzapine, and aortic banding. This method, previously recognized as a robust approach for creating an LHD-PH model, was further validated by our findings. Our results indicate that, compared to single-factor models, this multifactorial approach results in a higher incidence of PH. The LHD-PH mice exhibited increased left ventricular end-diastolic pressure (LVEDP), left heart remodeling, and pulmonary vascular remodeling, confirming the successful establishment of the model.

The development of PH-LHD is influenced by multiple factors, including left heart dysfunction, particularly diastolic dysfunction and elevated left atrial pressure, inflammation, oxidative stress, and genetic and genomic determinants. Among these, left heart dysfunction is the most critical factor. Increased pressure in the left ventricle and left atrium directly elevates pressure in the pulmonary veins and arteries, which constitutes the primary pathological mechanism of PH-LHD.[1] Elevated LVEDP and left heart remodeling are key contributors to the development of PH in the context of LHD. In heart failure with preserved ejection fraction (HFpEF), left ventricular hypertrophy and increased diastolic stiffness are commonly observed in association with hypertension and obesity.[19] Therefore, addressing left heart dysfunction, particularly left heart remodeling and fibrosis, is essential for managing PH-LHD. Several factors contribute to left heart remodeling and fibrosis, including β-adrenergic receptor signaling pathways, activation of the renin-angiotensin-aldosterone system (RAAS), calcium channels and calmodulin, oxidative stress, genetic and epigenetic influences, apoptosis, autophagy, and inflammatory responses.[20]

Among these factors, pericardial adipose tissue (PAT), a type of visceral fat located adjacent to the heart, plays a significant role in influencing cardiac structure and

FIGURE 4 RNA sequencing analysis of PAT in PH-LHD mice. (A) Heatmap of RNA-seq expression data showing 145 genes between the PH-LHD and control mice ($n = 3$). (B) volcano plot to show the DEGs between the PH-LHD and control mice. (C) Bubble plot to show GO-enriched items of DEGs. (D) Bubble plot to show KEGG-enriched items of DEGs. (E) PPI network of DEGs, among which Fasn, Acaca, Sftpc, and Scgb1a1 were the most closely connected.

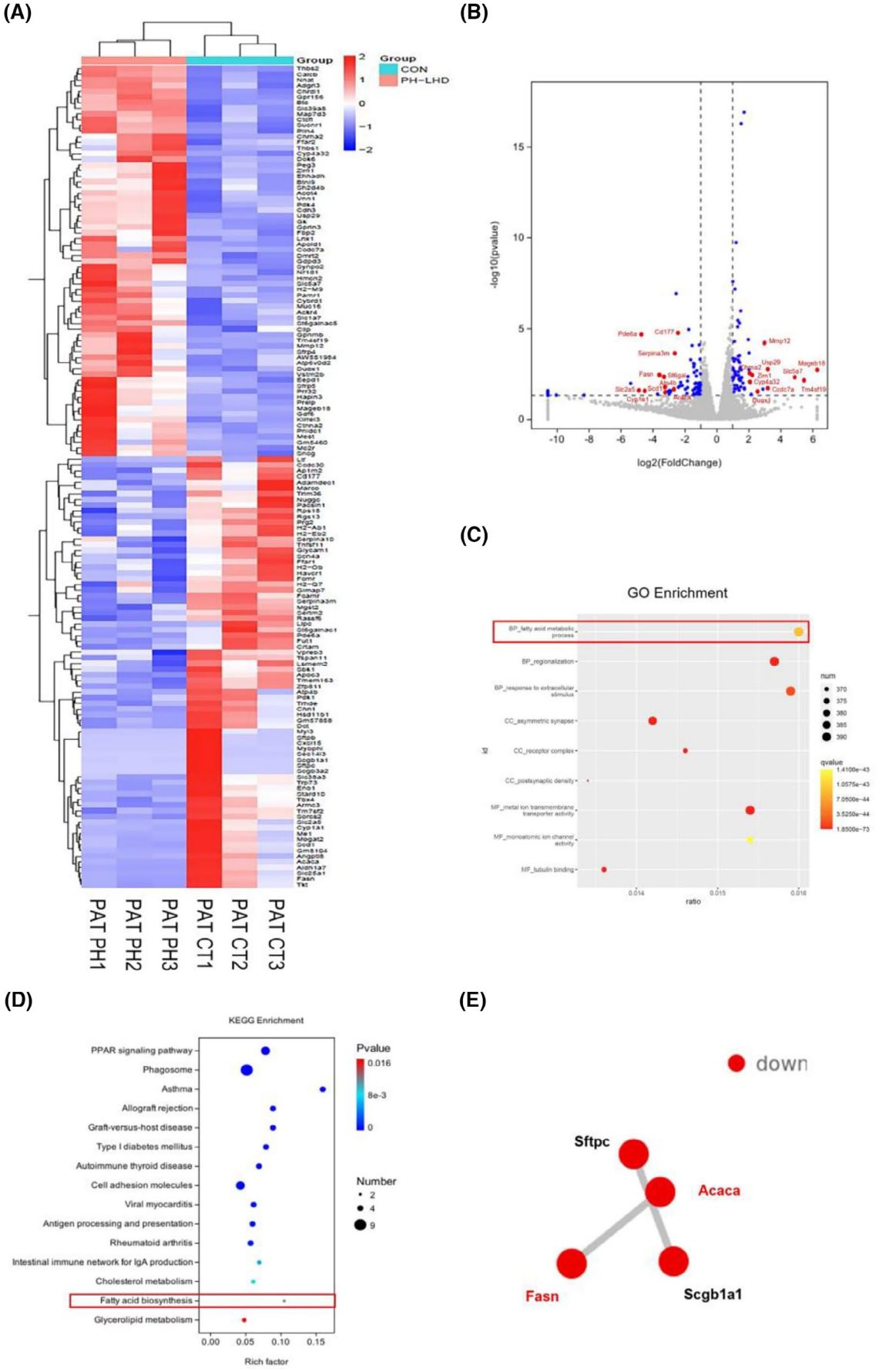
(A)
Group
CON
PH-LHD
PAT PH1
PAT PH2
PAT PH3
PAT CT1
PAT CT2
PAT CT3
(B)
-log10(pvalue)
log2(FoldChange)
(C)
GO Enrichment
BP_fatty acid metabolic process
BP_regionalization
BP_response to extracellular stimulus
CC_asymmetric synapse
CC_receptor complex
CC_postsynaptic density
MF_metal ion transmembrane transporter activity
MF_monoatomic ion channel activity
MF_tubulin binding
num
qvalue
ratio
(D)
KEGG Enrichment
PPAR signaling pathway
Phagosome
Asthma
Allograft rejection
Graft-versus-host disease
Type I diabetes mellitus
Autoimmune thyroid disease
Cell adhesion molecules
Viral myocarditis
Antigen processing and presentation
Rheumatoid arthritis
Intestinal immune network for IgA production
Cholesterol metabolism
Fatty acid biosynthesis
Glycerolipid metabolism
Pvalue
Number
Rich factor
(E)
down
Sftpc
Acaca
Fasn
Scgb1a1

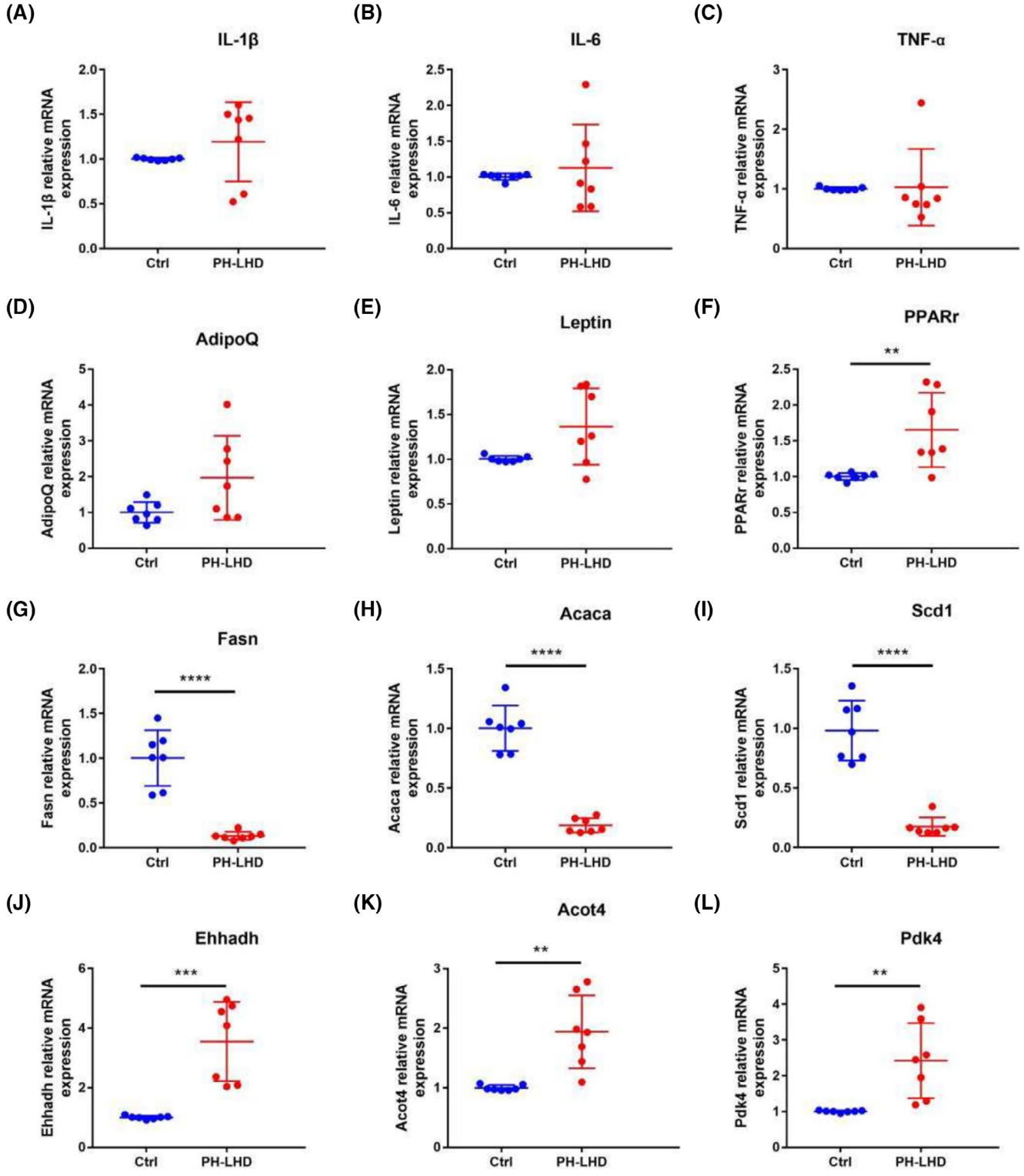

FIGURE 5 Impaired fatty acid synthesis and enhanced fatty acid breakdown in PAT of PH-LHD mice. (A–C) Quantitative analysis of relative mRNA expression of inflammatory factors, IL-1β, IL-6, and TNFα ($n = 7$). (D–F) Quantitative analysis of relative mRNA expression of adipokines, AdipoQ, Leptin, and PPARγ ($n = 7$). (G–L) Quantitative analysis of relative mRNA expression of key enzymes in fatty acid synthesis and metabolism, Fasn, Acaca, Scd1, Ehhadh, Acot4, and Pdk4 ($n = 7$). Acaca, acetyl-CoA carboxylase α; Acot4, acyl-CoA thioesterase 4; AdipoQ, adiponectin; Ehhadh, enoyl-CoA hydratase and 3-hydroxyacyl CoA dehydrogenase; Fasn, fatty acid synthase; IL-1β, interleukin 1β; IL-6, interleukin 6; Pdk4, pyruvate dehydrogenase kinase 4; PPARγ, peroxisome proliferator-activated receptor γ; Scd1, stearoyl CoA desaturase 1; TNFα, tumor necrosis factor. ****$p < .0001$, ***$p < .001$, **$p < .01$, PH-LHD vs. Ctrl group.

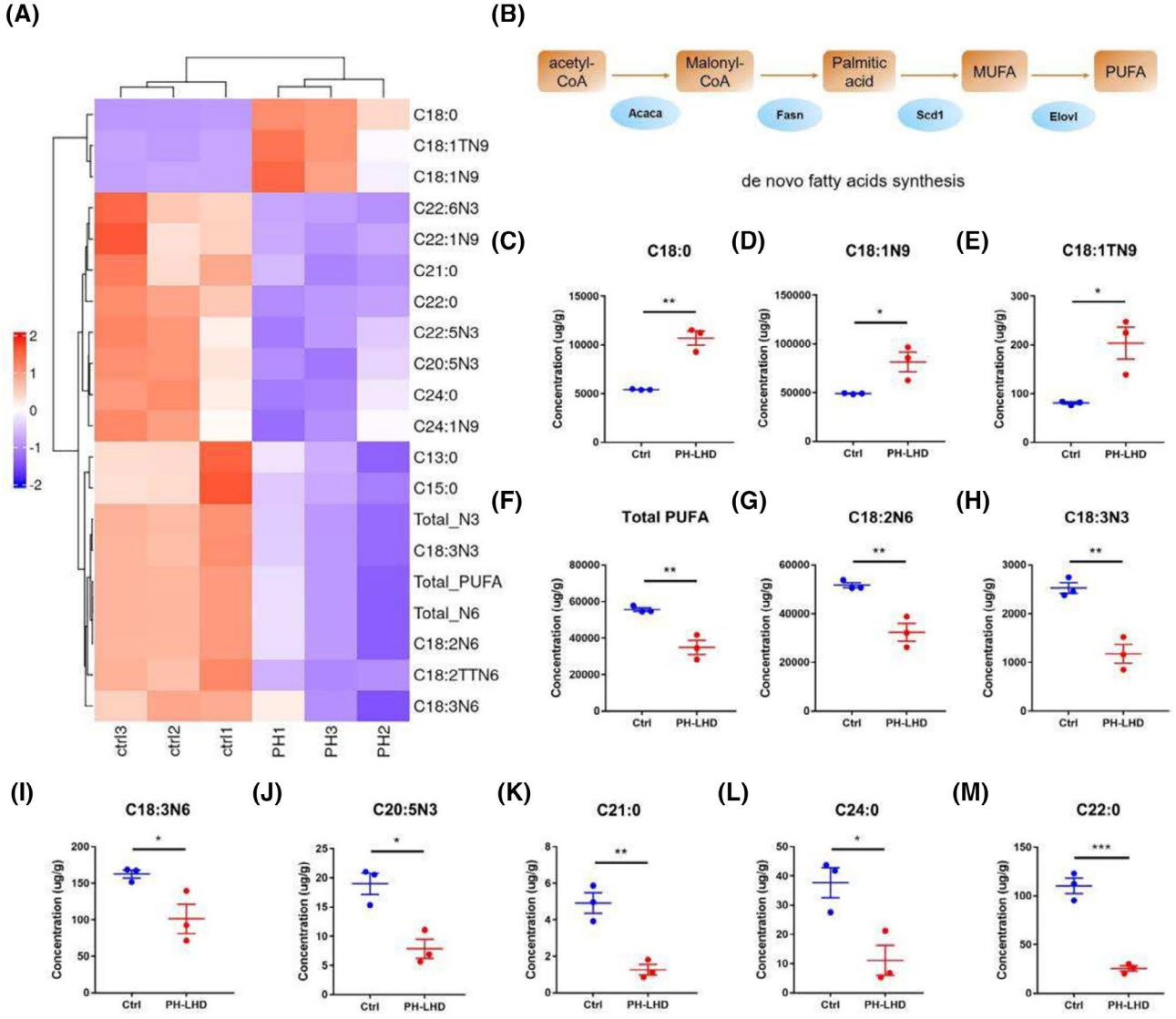

FIGURE 6 Distribution of medium- and long-chain fatty acids in PAT. (A) Heat map represents the content of different lipid species in the PAT of the control and PH-LHD mice. (B) Diagram of fatty acids de novo synthesis. (C–M) Levels of representative lipids in Control and PH-LHD mouse PAT ($n = 3$). MUFA, monounsaturated fatty acid; PUFA, polyunsaturated fatty acid. ***$p < .001$, **$p < .01$, *$p < .05$, PH-LHD vs. the control group.

function through various mechanisms. Notably, PAT levels were higher in the LHD-PH group compared to controls. Similarly, PAT is significantly increased in both high-fat diet (HFD)-induced and heart failure models.[21,22] PAT primarily exerts its effects on the heart through the secretion of adipokines, inflammatory mediators, intercellular communication, and modulation of fatty acid metabolism. Studies have demonstrated that PAT contributes to myocardial remodeling and fibrosis induced by HFD through adipokine secretion.[23] Additionally, PAT has been shown to regulate myocardial remodeling post-myocardial infarction (MI) via exosome-mediated signaling.[24] Furthermore, in a mouse model of pressure overload, PAT promotes progressive cardiac dilation, fibrosis, and transition to heart failure with reduced ejection fraction.[25]

Interestingly, although most studies suggest that PAT influences cardiac function primarily through adipokine and inflammation-related signaling pathways, our LHD-PH model did not show significant differences in these pathways. Instead, differentially expressed genes were enriched in fatty acid (FA) metabolism pathways, providing new insights into the underlying mechanisms. RT-PCR validation further confirmed that, in the LHD-PH group, there were no significant changes in adipokine or inflammatory factor expression in PAT compared to controls, but there were notable differences in FA metabolism.

Under physiological conditions, the myocardium primarily utilizes free fatty acids (FFAs) from coronary blood as its main energy substrate.[26] FFAs diffuse passively from areas of high concentration to low concentration within

the heart, PAT, and coronary arteries.[27] PAT acts as a metabolic buffer, absorbing FFAs and protecting the myocardium from the toxic effects of elevated fatty acid levels. Additionally, PAT serves as a lipid reservoir, directly supplying FFAs to the myocardium from epicardial fat.[28] It has been demonstrated that fatty acid-binding protein 4 in EAT facilitates the intracellular transport of FFAs from PAT to the myocardium.[29] Furthermore, PAT secretes vasoactive factors that modulate coronary artery tone, promoting FFA influx.[30,31]

These findings suggest that FA metabolism in PAT, particularly its role in supplying FFAs to the myocardium, is a crucial mechanism through which PAT affects cardiac function and structure. Overall, existing evidence indicates that PAT plays an active role in FA metabolism, characterized by high rates of FFA uptake and release, thereby providing FFAs as an energy source to the adjacent myocardium through fatty acid-binding protein mechanisms. However, the precise mechanisms by which PAT regulates FFA uptake and release, as well as their role in energy supply and potential tissue damage, remain to be fully elucidated. Further research is warranted to better understand these processes.

The uptake, synthesis, storage, and oxidative utilization of fatty acids are critical for maintaining normal cardiac function.[32,33] Our findings suggest that in the LHD-PH model, PAT demonstrates reduced de novo fatty acid synthesis and increased fatty acid catabolism, indicating an elevated release of FFAs and a diminished capacity of PAT to buffer fatty acids. These results align with those of Tang et al., who reported that both EAT and PAT in patients with CAD exhibited abnormal fatty acid metabolism, characterized by significant reductions in enzymes regulating fatty acid synthesis (such as FASN) and those involved in FFA oxidation.[34] Furthermore, our analysis of medium- and long-chain fatty acid composition in control and PH-LHD groups showed that, consistent with our RNA-seq and PCR data, most medium- and long-chain fatty acids, including polyunsaturated fatty acids (PUFAs), were decreased in the PH-LHD group, with only a few fatty acids, such as oleic acid, being elevated.

Oleic acid plays a crucial role in cardiac energy metabolism; within a physiological range, it serves as a key substrate for cardiac energy supply. However, the impact of oleic acid on the myocardium is largely dependent on the metabolic context.[35] In agreement with our findings, LINN et al. observed a significant increase in EAT oleic acid levels in patients with heart failure and type 2 diabetes mellitus, which may be related to elevated circulating oleic acid levels.[36] Additionally, we observed a decrease in the expression of most medium- and long-chain fatty acids in PH-LHD mice, potentially linked to the altered function of PAT and a metabolic shift from FFA oxidation to glycolysis.

In summary, our study provides new insights into the role of PAT in LHD-PH, highlighting the importance of fatty acid metabolism in PAT. However, further research is needed to elucidate these mechanisms, including studies on lipidomic changes in PAT and cardiac tissue. Moreover, the effects of different fatty acids in pathological states warrant investigation, including the dynamics of FFA alterations and lipid deposition in the heart.

There are limitations in this study that should be considered. One key limitation is that, while PAT has been the focus of our investigation, EAT has been more extensively studied in clinical research due to its close metabolic relationship with myocardial FFAs and its shared microcirculation with the myocardium. Notably, rodents possess PAT but lack EAT. Meanwhile, the body size, as well as the adipose tissue, is very small, and the anatomical structure is also very complex, which makes it impossible for us to use the simple EAT for research. However, studies suggest that in mice, PAT directly abuts the heart and may function similarly to EAT. Despite these similarities, further research is required to validate our findings in human tissues, which remains a priority for our future studies. Building on our current findings, we plan to explore in subsequent experiments whether increased fatty acids directly affect the pulmonary vasculature or primarily impact the left heart, thereby influencing the pulmonary vasculature through pressure transmission mechanisms. Furthermore, due to the multifactorial nature of our model, the incidence of PH is really high. Our analysis is based on comparisons between control groups and PH-LHD groups. It may be beneficial for us to further compare PH-LHD with models of left heart disease without PH, such as solely HFD or aortic banding, to better understand the specific impact of PAT on the occurrence and progression of PH. But the previous study has already verified the effects of these factors separately, determining that olanzapine and HFD-induced MetS combined with surgery-induced pressure overload achieve the most successful PH-LHD model.[12] Therefore, our study directly utilized the two-hit model.

AUTHOR CONTRIBUTIONS

JL designed the study, acquired funding, and administrated the project. HQ and WC performed the experiments. JC and ZM analyzed the data. HQ and JC drafted the manuscript. ZM, WC, LJ, YC, YT, and TW critically revised the manuscript and supervised the study. All authors contributed to the article and approved it final version of the manuscript for publication.

ACKNOWLEDGMENTS

This work was supported by the National Natural Science Foundation of China (Grant No. 82470055) and Hunan Provincial Natural Science Foundation of China (Grant No. 2022JJ30067 and No. 2023JJ40811). This work was supported by the Fundamental Research Funds for the Central Universities of Central South University (No. 2024ZZTS0534).

DISCLOSURES

The authors have declared that no conflict of interest exists.

DATA AVAILABILITY STATEMENT

The data that support the findings of this study are available in the Materials and Methods and Results of this article. The data for all analyses and figures are available upon request.

ORCID

Haihua Qiu https://orcid.org/0000-0002-0525-6238
Jiang Li https://orcid.org/0000-0003-4904-6635

REFERENCES

1. Guazzi M, Borlaug BA. Pulmonary hypertension due to left heart disease. *Circulation*. 2012;126(8):975-990.
2. Vachiéry JL, Tedford RJ, Rosenkranz S, et al. Pulmonary hypertension due to left heart disease. *Eur Respir J*. 2019;53(1):1801897.
3. Iorio A, Senni M, Barbati G, et al. Prevalence and prognostic impact of non-cardiac co-morbidities in heart failure outpatients with preserved and reduced ejection fraction: a community-based study. *Eur J Heart Fail*. 2018;20(9):1257-1266.
4. Miller WL, Grill DE, Borlaug BA. Clinical features, hemodynamics, and outcomes of pulmonary hypertension due to chronic heart failure with reduced ejection fraction: pulmonary hypertension and heart failure. *JACC Heart Fail*. 2013;1(4):290-299.
5. Lteif C, Ataya A, Duarte JD. Therapeutic challenges and emerging treatment targets for pulmonary hypertension in left heart disease. *J Am Heart Assoc*. 2021;10(11):e020633.
6. Guazzi M, Ghio S, Adir Y. Pulmonary hypertension in HFpEF and HFrEF: JACC review topic of the week. *J Am Coll Cardiol*. 2020;76(9):1102-1111.
7. Fitzgibbons TP, Czech MP. Epicardial and perivascular adipose tissues and their influence on cardiovascular disease: basic mechanisms and clinical associations. *J Am Heart Assoc*. 2014;3(2):e000582.
8. Si Y, Cui Z, Liu J, et al. Pericardial adipose tissue is an independent risk factor of coronary artery disease and is associated with risk factors of coronary artery disease. *J Int Med Res*. 2020;48(6):300060520926737.
9. Kim JS, Kim SW, Lee JS, et al. Association of pericardial adipose tissue with left ventricular structure and function: a region-specific effect? *Cardiovasc Diabetol*. 2021;20(1):26.
10. Koepp KE, Obokata M, Reddy YNV, Olson TP, Borlaug BA. Hemodynamic and functional impact of epicardial adipose tissue in heart failure with preserved ejection fraction. *JACC Heart Fail*. 2020;8(8):657-666.
11. Pugliese NR, Paneni F, Mazzola M, et al. Impact of epicardial adipose tissue on cardiovascular haemodynamics, metabolic profile, and prognosis in heart failure. *Eur J Heart Fail*. 2021;23(11):1858-1871.
12. Ranchoux B, Nadeau V, Bourgeois A, et al. Metabolic syndrome exacerbates pulmonary hypertension due to left heart disease. *Circ Res*. 2019;125(4):449-466.
13. Liu SF, Yan Y. Animal models of pulmonary hypertension due to left heart disease. *Animal Model Exp Med*. 2022;5(3):197-206.
14. Zacchigna S, Paldino A, Falcão-Pires I, et al. Towards standardization of echocardiography for the evaluation of left ventricular function in adult rodents: a position paper of the ESC working group on myocardial function. *Cardiovasc Res*. 2021;117(1):43-59.
15. Qiu H, Zhang Y, Li Z, et al. Donepezil ameliorates pulmonary arterial hypertension by inhibiting M2-macrophage activation. *Front Cardiovasc Med*. 2021;8:639541.
16. Huston JH, Shah SJ. Understanding the pathobiology of pulmonary hypertension due to left heart disease. *Circ Res*. 2022;130(9):1382-1403.
17. Obokata M, Reddy YNV, Pislaru SV, Melenovsky V, Borlaug BA. Evidence supporting the existence of a distinct obese phenotype of heart failure with preserved ejection fraction. *Circulation*. 2017;136(1):6-19.
18. Jasińska-Stroschein M. An updated review of experimental rodent models of pulmonary hypertension and left heart disease. *Front Pharmacol*. 2023;14:1308095.
19. Hieda M, Sarma S, Hearon CM Jr, et al. Increased myocardial stiffness in patients with high-risk left ventricular hypertrophy: the Hallmark of stage-B heart failure with preserved ejection fraction. *Circulation*. 2020;141(2):115-123.
20. Shah SJ, Borlaug BA, Kitzman DW, et al. Research priorities for heart failure with preserved ejection fraction: National Heart, Lung, and Blood Institute working group summary. *Circulation*. 2020;141(12):1001-1026.
21. Al-Dibouni A, Gaspar R, Ige S, et al. Unique genetic and histological signatures of mouse pericardial adipose tissue. *Nutrients*. 2020;12(6):1855.
22. Horckmans M, Bianchini M, Santovito D, et al. Pericardial adipose tissue regulates granulopoiesis, fibrosis, and cardiac function after myocardial infarction. *Circulation*. 2018;137(9):948-960.
23. Wang P, Luo C, Zhu D, et al. Pericardial adipose tissue-derived leptin promotes myocardial apoptosis in high-fat diet-induced obese rats through Janus kinase 2/reactive oxygen species/Na+/K+-ATPase signaling pathway. *J Am Heart Assoc*. 2021;10(18):e021369.
24. Man W, Song X, Xiong Z, et al. Exosomes derived from pericardial adipose tissues attenuate cardiac remodeling following myocardial infarction by Adipsin-regulated iron homeostasis. *Front Cardiovasc Med*. 2022;9:1003282.
25. Chen YW, Pat B, Gladden JD, et al. Dynamic molecular and histopathological changes in the extracellular matrix and inflammation in the transition to heart failure in isolated volume overload. *Am J Physiol Heart Circ Physiol*. 2011;300(6):H2251-60.

26. Lopaschuk GD, Ussher JR, Folmes CD, Jaswal JS, Stanley WC. Myocardial fatty acid metabolism in health and disease. *Physiol Rev*. 2010;90(1):207-258.
27. Iacobellis G, Barbaro G. Epicardial adipose tissue feeding and overfeeding the heart. *Nutrition*. 2019;59:1-6.
28. Nelson RH, Prasad A, Lerman A, Miles JM. Myocardial uptake of circulating triglycerides in nondiabetic patients with heart disease. *Diabetes*. 2007;56(2):527-530.
29. Vural B, Atalar F, Ciftci C, et al. Presence of fatty-acid-binding protein 4 expression in human epicardial adipose tissue in metabolic syndrome. *Cardiovasc Pathol*. 2008;17(6):392-398.
30. Marchington JM, Pond CM. Site-specific properties of pericardial and epicardial adipose tissue: the effects of insulin and high-fat feeding on lipogenesis and the incorporation of fatty acids in vitro. *Int J Obes*. 1990;14(12):1013-1022.
31. Sacks HS, Fain JN. Human epicardial fat: what is new and what is missing? *Clin Exp Pharmacol Physiol*. 2011;38(12):879-887.
32. van der Vusse GJ, van Bilsen M, Glatz JF. Cardiac fatty acid uptake and transport in health and disease. *Cardiovasc Res*. 2000;45(2):279-293.
33. Wende AR, Abel ED. Lipotoxicity in the heart. *Biochim Biophys Acta*. 2010;1801(3):311-319.
34. Tang Y, He Y, Li C, et al. RPS3A positively regulates the mitochondrial function of human periaortic adipose tissue and is associated with coronary artery diseases. *Cell Discov*. 2018;4:52.
35. Krieglstein J, Kewitz T, Kirchhefer U, et al. Damage of Guinea pig heart and arteries by a trioleate-enriched diet and of cultured cardiomyocytes by oleic acid. *PLoS One*. 2010;5(3):e9561.
36. Fosshaug LE, Dahl CP, Risnes I, et al. Altered levels of fatty acids and inflammatory and metabolic mediators in epicardial adipose tissue in patients with systolic heart failure. *J Card Fail*. 2015;21(11):916-923.

SUPPORTING INFORMATION

Additional supporting information can be found online in the Supporting Information section at the end of this article.

How to cite this article: Qiu H, Chen J, Mei Z, et al. Dysregulated fatty acid metabolism in pericardiac adipose tissue of pulmonary hypertension due to left heart disease mice. *The FASEB Journal*. 2025;39:e70355. doi:10.1096/fj.202402842R